 CMES, vol.29, no.1, pp.1-13, 2008

# A Rigid-fiber-based Boundary Element Model for Strength Simulation of Carbon Nanotube Reinforced Composites

**H. T. Wang[1] and Z. H. Yao[2]**

**Abstract:** Carbon nanotubes (CNTs) may provide ultimate enhancement in stiffness and strength for composite materials. This paper presents a rigid-fiber-based boundary integral equation formulation for the numerical simulation of debonding process and the corresponding strength of CNT reinforced composites. The CNT/matrix interfaces are assumed to fail when the interfacial shear force reaches a prescribed threshold, and the CNTs and matrix are considered to be detached in the failed areas. The matrix with one or several tens of originally well-bonded CNTs is subjected to an incremental tensile load and the effective stress-strain relations are readily obtained by the introduction of CNT/matrix debonding processes. An equivalent strength of CNT composites is also defined to study the effect of fracture process. In order to analyze considerable CNTs by use of the fast multipole method, a rigid-fiber-related preconditioning technique is introduced to deal with the case of CNT/matrix detachment. The boundary element model is solved on a desktop computer by using both the traditional GMRES solver and the fast multipole method. The impact of several micro-structural parameters on the debonding process and strength of CNT reinforced composites is discussed in the numerical tests, and some results are compared with experimental ones reported in the literature.

**Keyword:** boundary element; carbon nanotubes; composites; strength; fast multipole

[1] Corresponding author. Institute of Nuclear & New Energy Technology, Tsinghua University, Beijing, 100084, P. R. China. wanght@mail.tsinghua.edu.cn

[2] School of Aerospace, Tsinghua University, Beijing, 100084, P. R. China. demyzh@mail.tsinghua.edu.cn

## 1 Introduction

Carbon nanotubes (CNTs) have spurred considerable interest in recent years since their discovery by Iijima (1991), due to their unique mechanical, thermal and electrical properties (Popov 2004). CNTs are believed to have an extremely high Young's Modulus of 1TPa and tensile strength ranging from several tens to around 200GPa (Treacy, Ebbesen and Gibson 1996, Yu, Lourie, Dyer, Kelly and colleagues 2000, Demczyk, Wang, Cumings, Hetman and colleagues 2002). These characteristics make CNTs an ideal reinforcement to enhance the mechanical properties of those popularly used materials in various industrial applications (Andrews and Weisenberger 2004, Coleman, Khan, Blau and Gun'ko 2006). Much effort has been made to study the fabrication process of CNT/polymer composites (Thostenson and Chou 2002, Kimura, Ago, Tobita, Ohshima and colleagues 2002, Weisenberger, Grulke, Jacques, Rantell and Andrews 2003, Ko, Gogotsi, Ali, Naguib and colleagues 2003, Dalton, Collins, Munoz, Razal and colleagues 2003), and the experimental results of modulus and strength enhancement are continuously reported (Giannaris and Ajayan 1998, Shaffer and Windle 1999, Qian, Dickey, Andrews and Rantell 2000, Gong, Liu, Baskaran, Voise and colleagues 2000, Schadler, Thostenson and Chou 2003, Zhu and Narh 2004, Ryan, Cadek, Nicolosi, Blond and colleagues 2007). In addition, Increasing interest is being focused on the study of relations between the microstructures and effective properties of CNT-based composites by use of theoretical (Thostenson and Chou 2003, Odegard, Gates, Wise, Park and colleagues 2003) and numerical methods (Fisher, Bradshaw and Brinson 2003, Liu and Chen 2003, Chen and Liu 2004,

Ashrafi and Hubert 2006, Singh, Tanaka and Endo 2007, Chen, Cheng and Hsu 2007, Araujo and Gray 2008).

However, the reported mechanical properties of fabricated composites are diverse in the literature (Qian, Dickey, Andrews and Rantell 2000, Thostenson and Chou 2003, Bai and Allaoui 2003), and sometimes lower than predicted values (Odegard, Gates, Wise, Park and colleagues 2003). Numerous researchers have attributed these phenomena to the insufficient dispersion of CNTs (Odegard, Gates, Wise, Park and colleagues 2003, Bai and Allaoui 2003, Bai 2003) and variation of interfacial bonding forces between CNTs and the matrix (Weisenberger, Grulke, Jacques, Rantell and Andrews 2003, Bai 2003, Nan, Shi and Lin 2003, Ci and Bai 2006, Chen, Tao and Liu 2006). In some cases the pull-out of CNTs from the matrix is observed during the fracture process of the composites subjected to a tensile load (Ci and Bai 2006), indicating a lack of interfacial bondings; while the rupture of CNTs as a primary failure mode of the composites is also reported (Tao and Liu 2006), which demonstrates the existence of strong CNT/matrix interfaces. Both come to the fact that the interfacial stress plays an important role in the fracture process and the corresponding tensile strength of the CNT reinforced composites. In micro-mechanics, it is the interfacial shear stress that transfers the matrix load to the reinforcement. Attempt has been made to measure the pull-out force necessary to remove an individual multiwalled CNT embedded in polyethylene-butene using an AFM (Barber, Cohen and Wagner 2003), and an interfacial shear strength of 47MPa is reported.

The finite element method (FEM) has been successfully applied as a numerical tool to study the CNT/matrix interfacial forces based on continuum models. Such models commonly describe a matrix containing one or several well-bonded CNT fibers. As the fiber count increases, the computational cost might be a challenge for the FEM because a large number of volume meshes are generated due to the geometrically complicated CNT/matrix interfaces. On the other hand, the boundary element method (BEM) is deemed to be a potential candidate because only the CNT/matrix interfaces needed to be meshed. It has been demonstrated by several researchers that the predicted mechanical properties of composites by use of BEM agree well with the theoretical ones (Kong, Yao and Zheng 2002, Yao, Kong, Wang and Wang 2004). With the development of the fast multipole BEM (Greengard and Rokhlin 1997, Fu, Klimkowski, Rodin and colleagues 1998, Nishimura, Yoshida and Kobayashi 1999, Yoshida, Nishimura and Kobayashi 2001, Nishimura 2002, Aimi, Diligenti, Lunardini and Salvadori 2003, Nishimura and Liu 2004, Aoki, Amaya, Urago and Nakayama 2004, Chew, Song, Cui and colleagues 2004, Wang and Yao 2005, Liu, Nishimura, Otani, Takahashi and colleagues 2005, Shen and Liu 2007, Wang, Lei, Li, Huang and Yao 2007), it is possible to simulate large scale models with several hundred thousand unknowns on a desktop computer. Liu, Nishimura and Otani (2005) reported a large scale BEM model of CNT-based composites with 2000 aligned CNT fibers. While most research is still limited to the prediction of effective properties (elastic modulus, thermal conductivity, etc), there is little report on the numerical simulation of fracture process and strength of CNT-based composites. The BEM has realized successful simulation of interfacial stress distributions (Wang and Yao 2005, Liu, Nishimura, Otani, Takahashi and colleagues 2005, Liu, Nishimura and Otani 2005), which could be used on further study of the fracture process and strength simulation of such composites.

In this paper, a rigid-fiber-based boundary integral equation formulation is presented to simulate the mechanical properties of CNT reinforced composites with partly-attached CNT/matrix interfaces. The originally well-bonded interfaces are assumed to debond when the corresponding interfacial shear stress reach up to a prescribed threshold. The matrix model containing one or several tens of originally well-bonded CNTs is subjected to a unidirectional incremental tensile load and the effective nonlinear stress-strain relationship is obtained by taking into account the interfacial debonding processes. An equivalent

strength is also defined to study the effect of the fracture process. In order to implement the fast multipole BEM for large scale simulations, a rigid-fiber-related preconditioning technique is developed to deal with the case of CNT/matrix detachment. The BEM model is solved on a desktop computer by using both a conventional GMRES solver and a fast multipole method. The impact of several micro-structural parameters on the fracture process and the equivalent strength of CNT reinforced composites is discussed in the numerical tests, and some results are compared with experimental ones reported in the literature.

## 2 A rigid-fiber-based boundary integral equation formulation for partly-attached interfaces

The model of a matrix containing several partly-attached CNTs is shown in Fig. 1. Let $V_0$ denote the sub-domain of the matrix, $V_1, V_2, \ldots, V_k, \ldots, V_n$ the sub-domains of CNT fibers, $S_0$ the outer boundary of the matrix, and $S_k \equiv S_{k1} \cup S_{k2}, k = 1, \ldots, n$ the CNT/matrix interface of the $k$-th CNT fiber with the attached part $S_{k1}$ and detached part $S_{k2}$.

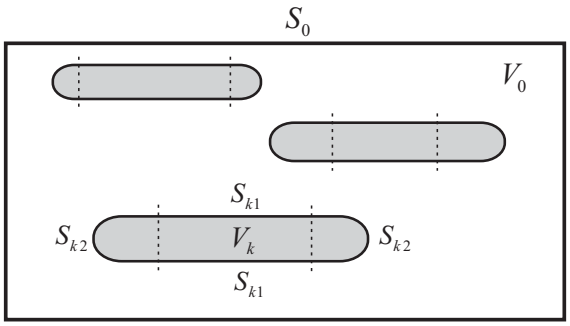


Figure 1: Model of a matrix containing several partly-attached CNTs

The boundary integral equations for 3D elasticity without body force are expressed for the matrix,

$$\frac{1}{2}u^0(x) + \int_{S_0+\sum S_{k1}+\sum S_{k2}} T^0(x,y)u^0(y)dS(y) = \int_{S_0+\sum S_{k1}+\sum S_{k2}} U^0(x,y)t^0(y)dS(y) \quad (1)$$

where $x$ and $y$ denote the source and field points on the boundary, respectively; $u^0(y)$ and $t^0(y)$ with superscript 0 representing the matrix are the boundary displacement and traction vectors at point $y$ respectively; $U^0(x,y)$ and $T^0(x,y)$ are the kernel functions of 3D elasticity,

$$\begin{aligned} U^0(x,y) &= \frac{1}{16\pi G(1-v)r}\left[(3-4v)\delta_{ij} + r_{,i}r_{,j}\right], \\ T^0(x,y) &= \frac{1}{8\pi(1-v)r^2}\left\{(1-2v)\left(r_{,j}n_i - r_{,i}n_j\right)\right. \\ &\quad \left. - \frac{\partial r}{\partial n}\left[(1-2v)\delta_{ij} + 3r_{,i}r_{,j}\right]\right\} \\ &\quad i,j = 1,2,3 \end{aligned} \quad (2)$$

with $r$ denoting the distance of $x$ and $y$, and $G$, $v$ being the shear modulus and Poisson's ratio, respectively. Note that $S_{k2}$ is detached part of the $k$-th CNT/matrix interface, which assumes both the $k$-th CNT and matrix boundaries in this part are free, that is, $t^0(y) = 0, y \in S_{k2}$. In addition, considering the fact that tensile modulus of a CNT (1TPa) is usually several orders of magnitude higher than that of the matrix (Liu, Nishimura and Otani 2005), it is reasonable to assume a CNT to be rigid, with a rigid-body-mode displacement of $u^k(y)$ expressed as,

$$u^k(y) = d^k + w^k \times p^k(y), y \in S_k \quad (3)$$

Where $d^k$ is the rigid-body-mode translational displacement vector, $w^k$ the rotational vector, and $p^k(y)$ the position vector from the center of the $k$-th CNT to point $y$. Considering $u^k(y) = u^0(y)$ at the attached part $S_{k1}$ and free boundary conditions at $S_{k2}$, Eq. (1) is rewritten as,

$$\begin{aligned} &\frac{1}{2}u^0(x) + \int_{S_0} T^0(x,y)u^0(y)dS(y) \\ &+ \int_{\sum S_k} T^0(x,y)u^k(y)dS(y) \\ &+ \int_{\sum S_{k2}} T^0(x,y)\overline{u}^k(y)dS(y) \\ &\qquad = \int_{S_0+\sum S_{k1}} U^0(x,y)t^0(y)dS(y) \end{aligned} \quad (4)$$

Where $\overline{u}^k(y) = u^0(y) - u^k(y)$. The second integral containing the traction kernel functions and

rigid-body-mode displacement can be deduced into simple forms according to Liu, Nishimura, Otani, Takahashi and colleagues (2005),

$$\begin{aligned} &\int_{S_k} T^0(x,y)u^k(y)dS(y) = \frac{1}{2}u^k(x), \quad x \in S_k \\ &\int_{S_k} T^0(x,y)u^k(y)dS(y) = 0, \quad x \notin S_k \end{aligned} \tag{5}$$

Substituting Eqs. (3) and (5) into Eq. (4), one obtains various formulations in three cases.

**Case 1.** for $x \in S_0$,

$$\begin{aligned} &\frac{1}{2}u^0(x) + \int_{S_0} T^0(x,y)u^0(y)dS(y) \\ &+ \int_{\sum S_{k2}} T^0(x,y)\overline{u}^k(y)dS(y) \\ &\qquad = \int_{S_0+\sum S_{k1}} U^0(x,y)t^0(y)dS(y) \end{aligned} \tag{6}$$

**Case 2.** for $x \in S_{k1}$, $k = 1,\ldots,n$,

$$\begin{aligned} &d^k + w^k \times p^k(x) + \int_{S_0} T^0(x,y)u^0(y)dS(y) \\ &+ \int_{\sum S_{k2}} T^0(x,y)\overline{u}^k(y)dS(y) \\ &\qquad = \int_{S_0+\sum S_{k1}} U^0(x,y)t^0(y)dS(y) \end{aligned} \tag{7}$$

**Case 3.** for $x \in S_{k2}$, $k = 1,\ldots,n$,

$$\begin{aligned} &d^k + w^k \times p^k(x) + \frac{1}{2}\overline{u}^k(x) \\ &+ \int_{S_0} T^0(x,y)u^0(y)dS(y) \\ &+ \int_{\sum S_{k2}} T^0(x,y)\overline{u}^k(y)dS(y) \\ &\qquad = \int_{S_0+\sum S_{k1}} U^0(x,y)t^0(y)dS(y) \end{aligned} \tag{8}$$

Let $S_0^U$ and $S_0^T$ denote boundaries of $S_0$with given displacement and traction, respectively, $S_0 = S_0^U \cup S_0^T$. There are three groups of unknowns according to Eqs. (6) to (8): $u^0(y)$ on $S_0^T$ and $t^0(y)$ on $S_0^U + \sum S_{k1}$; $\overline{u}^k(y)$ on $\sum S_{k2}$; $d^k$ and $w^k$ for the rigid-body motion of the $k$-th CNT fiber. The first and second groups cover the entire boundaries including outer boundary of the matrix and CNT/matrix interfaces; the last group needs additional equations, which could be obtained by considering the force and moment equilibrium of the $k$-th CNT,

$$\int_{S_{k1}} t^0(y)dS(y) = 0 \tag{9}$$

$$\int_{S_{k1}} p^k(y) \times t^0(y)dS(y) = 0 \tag{10}$$

Eqs. (6-10) are solved simultaneously to obtain all the three groups of unknowns, in which $t^0(y)$ on $\sum S_{k1}$ can be used to determine the status of CNT/matrix interfacial bonding. The BEM is employed to solve the corresponding equation systems. Commonly used solvers are direct LU decomposition, iterative GMRES, and the fast multipole method (FMM). The FMM has been successfully applied to simulate 2D and 3D models containing a large number of inclusions or cracks with computational cost of $O(N)$, where $N$ is the number of boundary unknowns. Interested readers can refer to Fu, Klimkowski, Rodin and colleagues (1998), Nishimura, Yoshida and Kobayashi (1999), Yoshida, Nishimura and Kobayashi (2001), Nishimura (2002), Nishimura and Liu (2004), Wang and Yao (2005), Liu, Nishimura, Otani, Takahashi and colleagues (2005), Shen and Liu (2007) for detailed discussions.

## 3 Procedures for simulation of CNT/matrix debonding process

Real fracture process of CNT reinforced composites is complicated, including the CNT/matrix debonding, CNT break, matrix rupture and other interaction factors. To begin with, only the CNT/matrix debonding process, which has been observed from numerous experiments and deemed to dominate the fracture process in some cases (Ci and Bai 2006), is taken into consideration in this study.

### *3.1 Debonding criterion*

In micro-mechanics, the CNT/matrix interfacial shear stresses contribute to the load transfer from the matrix to CNTs. Assume a shear stress threshold $\overline{\tau}_c$, and the originally well-bonded CNT/matrix interfaces are considered to

be debonded when the interfacial shear stresses reach above $\overline{\tau}_c$. In addition, rebonding is not allowed in the debonded areas during the simulation of the fracture process.

### 3.2 Simulation procedures

Consider a matrix model containing numerous originally well-bonded CNTs subjected to a unidirectional incremental displacement load. The procedures of CNT/matrix debonding are as follows.

**Step 1.** For an initial unidirectional displacement load $F_0$, perform a BEM analysis and obtain the maximum interfacial shear stress $\tau_{\max}$; define an amplification factor $a_{amp} = \tau_{\max}/\overline{\tau}_c$; and reset $F_0 = F_0/\ a_{amp}$. For $k = 1\sim N$:

**Step 2.** Define a unidirectional displacement $F = F_0 + k\Delta_F$, where $\Delta_F$ is a prescribed value of load increment, and perform a BEM analysis to obtain the shear stresses of all boundary elements on the CNT/matrix interfaces;

**Step 3.** For those interfacial elements that are bonded before and have a value of shear stress larger than $\overline{\tau}_c$, set flags of these elements to be debonded in order to simulate interfacial debonding;

**Step 4.** if there exist interfacial elements with changed flags from bonding to debonding in Step 3, go to Step 2; otherwise go ahead;

**Step 5.** Calculate the effective stress, strain, Young's Modulus and the ratio of debonded areas to the whole interfaces.

Although a linear analysis is performed in each incremental step, a nonlinear stress-strain curve will be obtained finally.

### 3.3 Equivalent strength

An equivalent stress $\sigma_{eq}$ is defined in order to study the impact of the interfacial debonding: $\sigma_{eq}$ equals to the effective stress when the effective Young's Modulus $E$ reaches that of the matrix $E_m$ during the simulation of debonding process.

## 4 Rigid-fiber-based preconditioner for fast multipole BEM

In order to implement the fast multipole BEM, a rigid-fiber-related preconditioner is developed to deal with the effect of CNT/matrix debonding. In this study, we consider a left preconditioner denoted by $M$, and the preconditioned equation systems from Eqs. (6-10) becomes,

$$(MA)X = MB \tag{11}$$

Generally speaking, $M$ should be selected to be an approximation of the inversion of the coefficient matrix $A$ in Eq. (11). As $A$ is not explicitly available for the fast multipole BEM, let $\overline{A}$ denote a diagonal form of $A$,

$$\overline{A} = \begin{bmatrix} A_0 & 0 & 0 & \cdots & 0 & 0 & 0 & \cdots & 0 \\ 0 & A_1 & 0 & \cdots & 0 & E_1 & 0 & \cdots & 0 \\ 0 & 0 & A_2 & \cdots & 0 & 0 & E_2 & \cdots & 0 \\ \vdots & \vdots & \vdots & \ddots & \vdots & \vdots & \vdots & \ddots & \vdots \\ 0 & 0 & 0 & \cdots & A_n & 0 & 0 & \cdots & E_n \\ 0 & F_1 & 0 & \cdots & 0 & 0 & 0 & \cdots & 0 \\ 0 & 0 & F_2 & \cdots & 0 & 0 & 0 & \cdots & 0 \\ \vdots & \vdots & \vdots & \ddots & \vdots & \vdots & \vdots & \ddots & \vdots \\ 0 & 0 & 0 & \cdots & F_n & 0 & 0 & \cdots & 0 \end{bmatrix} \tag{12}$$

Where $A_0$ is a block-diagonal matrix with total $l$ diagonal blocks, where $l$ is the count of tree leaves of the fast multipole method. Each diagonal block of $A_0$ arises from the boundary elements of the outer surface of the matrix contained in a corresponding tree leaf (Wang, Yao and Wang 2005). $A_k$, $k = 1,\ldots,n$ is a sub-matrix arising from the boundary elements of the $k$-th CNT fiber. $E_k$, $k = 1,\ldots,n$ is related to the rigid-body motion of the $k$-th CNT fiber, and $F_k$, $k = 1,\ldots,n$ is related to the force and moment equilibrium of the $k$-th

CNT fiber. The forms of $E_k$ and $F_k$ are,

$$E_k = \begin{bmatrix} a_1 \\ a_2 \\ \vdots \\ a_m \end{bmatrix},$$
$$a_i = \begin{bmatrix} 1 & 0 & 0 & 0 & p_3 & -p_2 \\ 0 & 1 & 0 & -p_3 & 0 & p_1 \\ 0 & 0 & 1 & p_2 & -p_1 & 0 \end{bmatrix}, \quad (13)$$
$$i = 1, \ldots, m$$

$$F_k = \begin{Bmatrix} a_1^T S_1 & a_2^T S_2 & \cdots & a_{m_1}^T S_{m_1} & 0 & \cdots & 0 \end{Bmatrix} \quad (14)$$

With $p_i = \begin{Bmatrix} p_1 & p_2 & p_3 \end{Bmatrix}$ being the position vector for the $i$-th element of the $k$-th CNT fiber, $m$ and $m_1$ the counts of total and bonded interfacial elements of the $k$-th CNT fiber, respectively, and $S_i$, $i$ = 1,..., $m_1$ the area of the $i$-th bonded interfacial element of the $k$-th CNT fiber.

$\overline{A}$ coincides with the idea of fast multipole BEM. After $\overline{A}$ is constructed, we define $M$ to be $\overline{A}^{-1}$,

$$M = \begin{bmatrix} M_0 & 0 & 0 & \cdots & 0 & 0 & 0 & \cdots & 0 \\ 0 & M_1 & 0 & \cdots & 0 & U_1 & 0 & \cdots & 0 \\ 0 & 0 & M_2 & \cdots & 0 & 0 & U_2 & \cdots & 0 \\ \vdots & \vdots & \vdots & \ddots & \vdots & \vdots & \vdots & \ddots & \vdots \\ 0 & 0 & 0 & \cdots & M_n & 0 & 0 & \cdots & U_n \\ 0 & V_1 & 0 & \cdots & 0 & W_1 & 0 & \cdots & 0 \\ 0 & 0 & V_2 & \cdots & 0 & 0 & W_2 & \cdots & 0 \\ \vdots & \vdots & \vdots & \ddots & \vdots & \vdots & \vdots & \ddots & \vdots \\ 0 & 0 & 0 & \cdots & V_n & 0 & 0 & \cdots & W_n \end{bmatrix} \quad (15)$$

Where,

$$M_0 = (A_0)^{-1},$$
$$\begin{bmatrix} M_k & U_k \\ V_k & W_k \end{bmatrix} = \begin{bmatrix} A_k & E_k \\ F_k & 0 \end{bmatrix}^{-1}, \quad k = 1, \ldots, n \quad (16)$$

## 5 Numerical results

The developed BEM code runs on a desktop computer with a processor AMD 2800+ and memory of 1GB. The programming language is C++. The impact of several micro-structural parameters, namely the CNT aspect ratio, volume fraction and CNT count on the interfacial debonding process and the equivalent strength is studied.

### 5.1 Computational model

CNTs are treated as effective straight fibers with infinitely large modulus. The aspect ratio $\alpha$ of a CNT fiber is defined as,

$$\alpha = L/D \quad (17)$$

With $L$ and $D$ being length and diameter of the CNT fiber, respectively. The matrix cube has dimensions of $l_x \times l_y \times l_z$. The volume fraction $c$ of CNTs is defined as,

$$c = nV_{CNT}/V_{MAT} \quad (18)$$

With $V_{CNT}$ and $V_{MAT}$ being volumes of a CNT and the matrix, respectively, and $n$ the CNT count.

Triangular constant boundary elements are employed in discretization of the surface of both CNT/matrix interfaces and outer matrix surfaces. Total 4 values of CNT fiber aspect ratio are taken into consideration: 5, 10, 20 and 40. Fig. 2 shows these 4 meshed fibers with various aspect ratios. Fig. 3 shows a meshed cubic matrix with $l_x : l_y : l_z = 10 : 1 : 1$. Fig. 4 shows a matrix containing several tens of aligned CNT fibers.

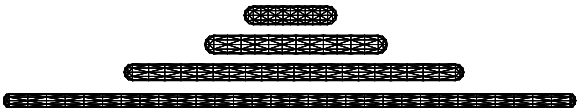

Figure 2: Meshed CNT fibers with aspect ratio of 5, 10, 20, 40

### 5.2 Variation of CNT aspect ratio

In this example, a matrix with one CNT fiber in the center is simulated by use of BEM with traditional GMRES solver, and the impact of CNT aspect ratio on the CNT/matrix interfacial debonding process and equivalent strength is studied. Young's Modulus of the matrix $E_m$ = 2.4GPa. The threshold of interfacial shear stress $\tau_c$ = 47MPa. The volume fraction of CNTs equals to 2.7%.

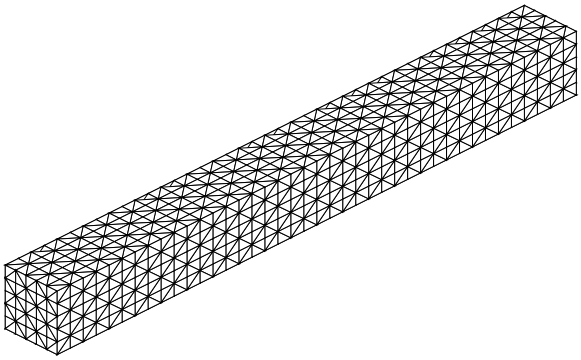

Figure 3: Meshed cubic matrix

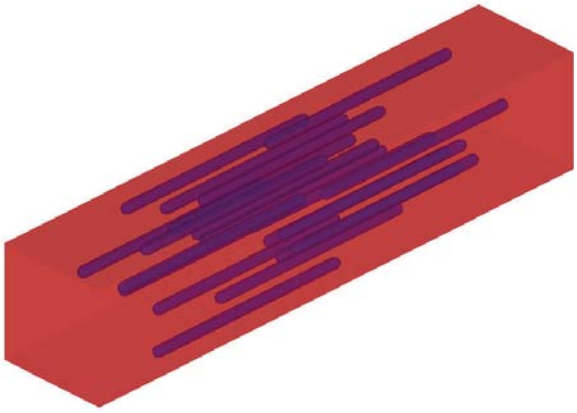

Figure 4: A matrix containing multiple aligned CNTs

Figs. 5 and 6 show examples of debonding processes of CNTs with aspect ratio of 10 and 20, respectively (matrix: red color, attached interface: blue, detached interface: green). Fig. 7 shows the nonlinear stress-strain curves, Fig. 8 shows the effective Young's Modulus versus tensile stress, Fig. 9 shows the ratio of bonded / entire interfacial area versus the strain, and Fig. 10 shows iterations in each incremental step in the case of aspect ratio equal to 40.

It is shown from Figs. 5 to 8 that CNTs with higher aspect ratio lead to a better enhancement of elastic modulus, while result in a start of debonding process at a smaller strain/stress. For the CNT with aspect ratio of 10, the effective Young's Modulus (around 3.2GPa) before debonding occurs is very close to the experimental data (around 3.3GPa) of multi-walled carbon nanotube/polymer composites reported by Thostenson (2003) (In his paper, the WMNT volume fraction of 2.7% refers to the WMNT weight fraction of 5%). While for CNTs with other values of aspect ratio, there is a large discrepancy between the simulated values and the experimental data. A dramatic enhancement is achieved for the case of CNTs with aspect ratio of 40, which is still much less than typical values of aspect ratio of real CNTs. The discrepancy may be attributed to the fact that real CNTs are always curved rather than straight, and poor dispersion is commonly observed resulting in a decrease of the effect of CNT enhancement. It is also shown that the equivalent strength under various aspect ratios seem to converge to a value around 23 MPa, which indicates aspect ratio of the rigid-fiber model has little impact on the equivalent strength.

The reduction of debonded areas in Fig. 9 indicates that even though the CNTs with higher aspect ratio begin to debond at a lower strain, the debonding speed is relatively slower at the original debonding process. Fig. 10 shows the iterations that are needed in each incremental step is typically less than 10.

### *5.3 Variation of CNT volume fraction*

In this example, a matrix with one CNT fiber in the center is simulated by use of BEM with traditional GMRES solver, and the impact of fiber volume fraction on the debonding process and equivalent strength is studied. The CNT aspect ratio is fixed to be 20. Young's Modulus of the matrix $E_m$ = 2.4GPa. The threshold of interfacial shear stress $\tau_c = 47$MPa. The volume fraction of CNTs equals varies between 1%, 2.7%, 5.5% and 10%. Fig. 11 shows the nonlinear stress-strain curves, and Fig. 12 shows the effective Young's Modulus versus tensile stress.

It is shown that CNTs with higher volume fraction lead to a better enhancement of the effective elastic modulus and result in a larger stress when debonding process begins. While the start strain seems to be insensitive to the CNT volume fraction. The equivalent strength is distributed ranging from 15MPa to around 26MPa, and a higher

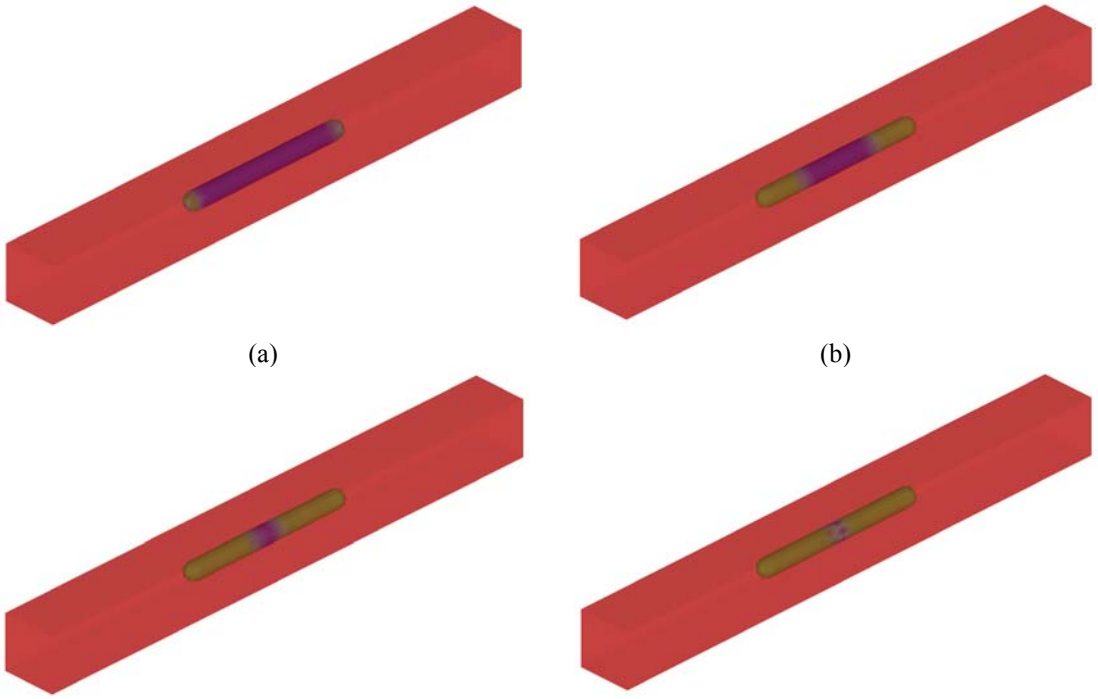

(a) (b)

(c) (d)

Figure 5: Debonding processes of CNT/matrix interfaces (CNT aspect ratio: 10)

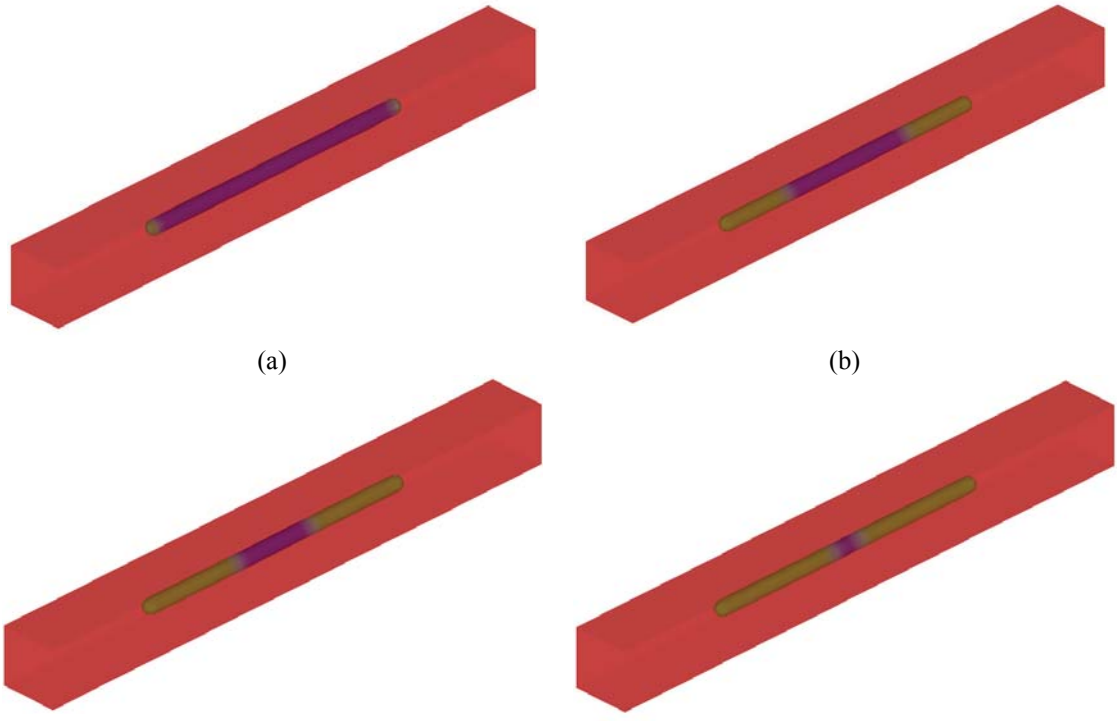

(a) (b)

(c) (d)

Figure 6: Debonding processes of CNT/matrix interfaces (CNT aspect ratio: 20)

CNT volume fraction leads to a higher equivalent strength, which coincides with typical observations in the experiments.

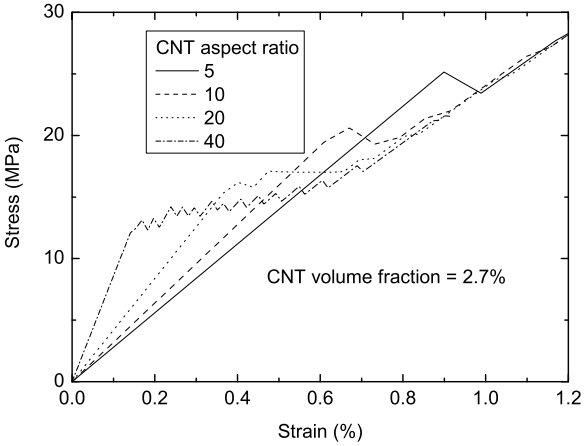


Figure 7: Stress versus strain with various CNT aspect ratios

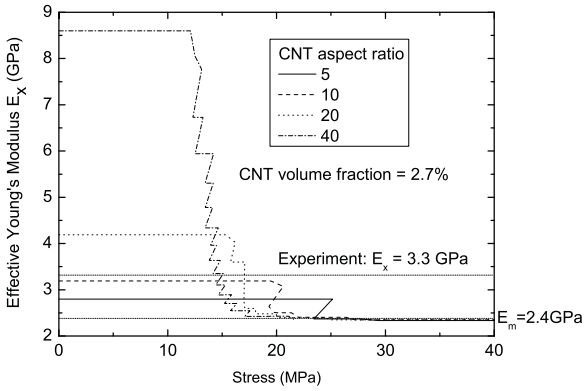


Figure 8: Effective Young's Modulus versus stress with various CNT aspect ratios

### *5.4 Variation of CNT count by use of fast multipole BEM*

In this example, a matrix containing 20 aligned and randomly distributed CNT fibers is simulated by use of BEM with a new version of fast multipole BEM solver, and the impact of CNT count on the debonding process and equivalent strength is studied. The CNT aspect ratio is fixed to be 20. Young's Modulus of the matrix $E_m = 2.4$GPa. The threshold of interfacial shear stress $\tau_c = 47MPa$. The volume fraction of CNTs equals 5.5%. The

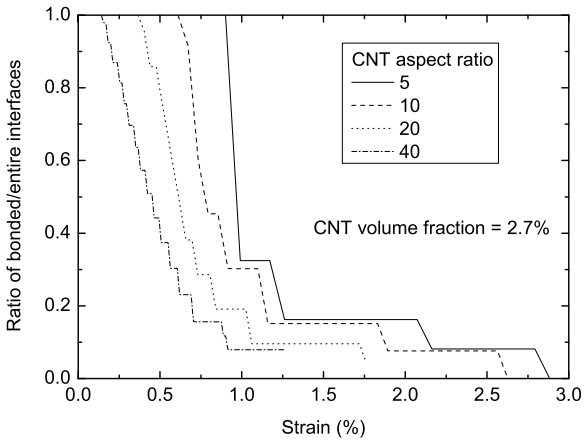


Figure 9: Ratio of bonded / entire area versus strain with various CNT aspect ratios

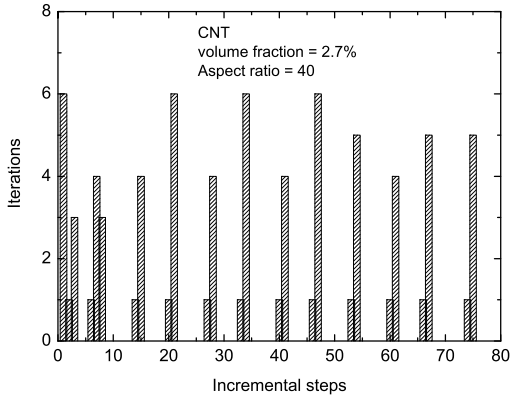


Figure 10: Iterations version incremental steps (CNT aspect ratio: 40)

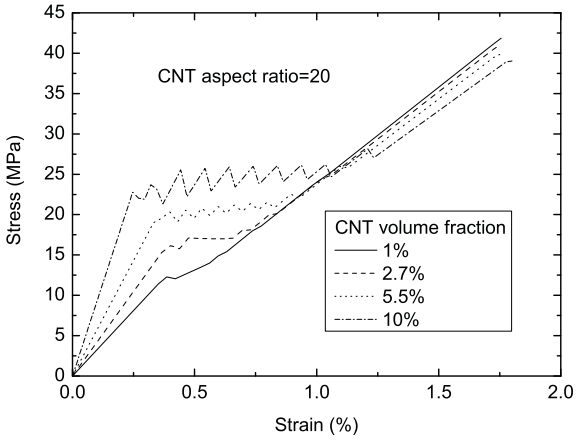


Figure 11: Stress versus strain with various CNT volume fractions

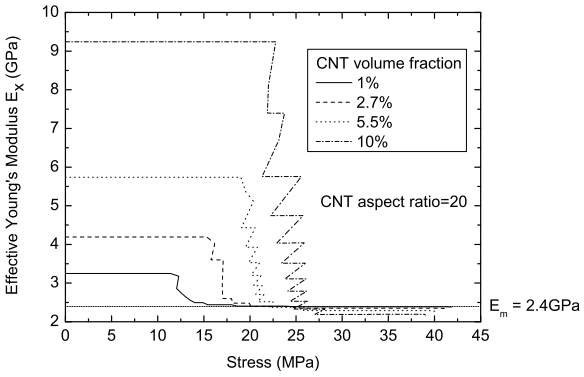


Figure 12: Effective Young's Modulus versus stress with various CNT volume fractions

model is shown in Fig. 4, and Fig. 13 shows interfacial debonding distributions of these 20 CNT fibers near the end of simulation when most interfacial elements are debonded. Fig. 14 shows the nonlinear stress-strain curves, and Fig. 15 shows the effective Young's Modulus versus tensile stress.

It is clearly shown that debonding processes of CNTs are strongly impacted by interaction forces, and result in an irregular figure of detachment for each CNT fiber. The final bonded areas are concentrated in the center of the model with similar axial coordinate values. This phenomenon is due to the fact that debonding process of one CNT fiber will result in a high stress concentration at other CNTs around it, and lead to new debonding processes following its debonding along the axial direction. Large CNT count result in a smooth stress-strain curve and a smaller strain/stress when debonding process begins. While the effective Young's modulus before debonding occurs and the final equivalent stress are insensitive to the CNT count.

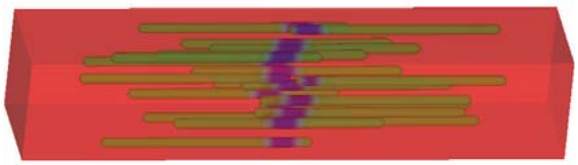

Figure 13: Debonding processes of CNT/matrix interfaces (CNT count: 20)

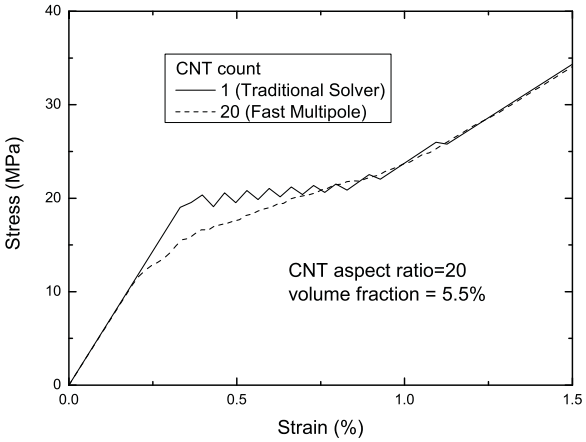


Figure 14: Stress versus strain with various CNT count

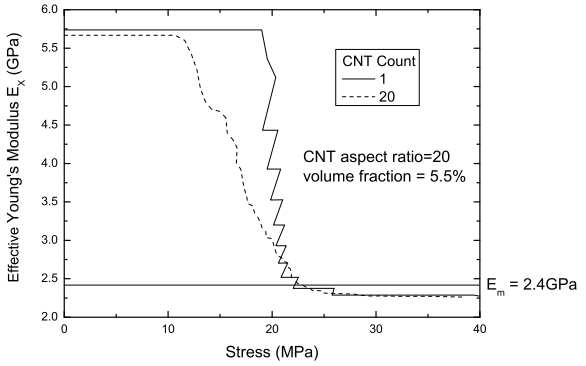


Figure 15: Effective Young's Modulus versus stress with various CNT count

## 6 Conclusions

A rigid-fiber-based boundary integral equation formulation is developed to simulate the interfacial debonding process of CNT reinforced composites. An equivalent strength is defined to study the impact of detaching process on the fracture and final strength of such composites. Numerical tests discuss the effects of various microstructural parameters on the debonding process and the corresponding equivalent strength. The results clearly demonstrate the efficiency of the proposed method for the simulation of interfacial debonding process. The comparison with experimental data of CNT composites indicates a potential application of this method to the mechanical analysis of CNT composites.

Due to the limited computer resources and huge time cost, the meshes for both CNTs and matrix are coarse. It is necessary in the future to perform further sensitivity analysis of several parameters. In addition, the possibility of CNT breaks will be taken into consideration in the near future, which would make the numerical simulation closer to the real fracture process of CNT-based composites.

**Acknowledgement:** Financial support for the project from the National Natural Science Foundation of China, under grant No. 10602029 is gratefully acknowledged.

## References

**Aimi, A.; Diligenti, M.; Lunardini, F.; Salvadori, A.** (2003): A new application of the panel clustering method for 3D SGBEM. *CMES: Computer Modeling in Engineering & Sciences*, vol. 4, no. 1, pp. 31–49.

**Andrews, R.; Weisenberger, M. C.** (2004): Carbon nanotube polymer composites. *Current Opinion in Solid State and Materials Science*, vol. 8, pp. 31–37.

**Aoki, S.; Amaya, K.; Urago, M.; Nakayama, A.** (2004): Fast multipole boundary element analysis of corrosion problems. *CMES: Computer Modeling in Engineering & Sciences*, vol. 6, no. 2, pp. 123–131.

**Ashrafi, B.; Hubert, P.** (2006): Modeling the elastic properties of carbon nanotube array/polymer composites. *Composites Science and Technology*, vol. 66, no. 3-4, pp. 387–396.

**Araujo, F. C.; Gray, L. J.** (2008): Evaluation of effective material parameters of CNT-reinforced composites via 3D BEM. *CMES: Computer Modeling in Engineering & Sciences*, vol. 24, no. 2-3, pp. 103–121.

**Bai, J. B.; Allaoui, A.** (2003): Effect of the length and the aggregate size of MWNTs on the improvement efficiency of the mechanical and electrical properties of nanocomposites – experimental investigation. *Composites: Part A*, vol. 34, pp. 689–694.

**Bai, J. B.** (2003): Evidence of the reinforcement role of chemical vapour deposition multi-walled carbon nanotubes in a polymer matrix. *Carbon*, vol. 41, no. 6, pp. 1325–1328.

**Barber, A. H.; Cohen, S. R.; Wagner, H. D.** (2003): Measurement of carbon nanotube-polymer interfacial strength. *Appl Phys Lett*, vol. 82, no. 23, pp. 4140–4142.

**Chen, W.; Tao, X. M.; Liu, Y. Y.** (2006): Carbon nanotube-reinforced polyurethane composite fibers. *Composites Science and Technology*, vol. 66, no. 15, pp. 3029–3034.

**Chen, W. H.; Cheng, H. C.; Hsu, Y. C.** (2007): Mechanical properties of carbon nanotubes using molecular dynamics simulations with the inlayer van der Waals interactions. *CMES: Computer Modeling in Engineering & Sciences*, vol. 20, no. 2, pp. 123–145.

**Chen, X. L.; Liu, Y. J.** (2004): Square representative volume elements for evaluating the effective material properties of carbon nanotube-based composites. *Comput Mater Sci*, vol. 29, no. 1, pp. 1–11.

**Chew, W. C.; Song, J. M.; Cui, T. J.; Velarnparambil, S; Hastriter, M. L.; Hu, B.** (2004): Review of large scale computing in electromagnetics with fast integral equation solvers. *CMES: Computer Modeling in Engineering & Sciences*, vol. 5, no. 4, pp. 361–372.

**Ci, L. J.; Bai, J. B.** (2006): The reinforcement role of carbon nanotubes in epoxy composites with different matrix stiffness. *Composites Science and Technology*, vol. 66, pp. 599–603.

**Coleman, J. N.; Khan, U.; Blau, W. J.; Gun'ko, Y. K.** (2006): Small but strong: A review of the mechanical propertie of carbon nanotube–polymer composites. *Carbon*, vol. 44, pp. 1624–1652.

**Dalton, A. B.; Collins, S.; Munoz, E.; Razal, J. M.; Ebron, V. H.; Ferraris, J. P.; Coleman, J. N.; Kim, B. G.; Baughman, R. H.** (2003): Super-tough carbon-nanotube fibres - These extraordinary composite fibres can be woven into electronic textiles. *Nature*, vol. 423, no. 6941, pp. 703–703.

**Demczyk, B. G.; Wang, Y. M.; Cumings, J.; Hetman, M.; Han, W.; Zettl, A.; Ritchie, R.**

**O.** (2002): Direct mechanical measurement of the tensile strength and elastic modulus of multiwalled carbon nanotubes. *Mater Sci Eng*, vol. A334, no. 12, pp. 173–178.

**Fisher, F. T.; Bradshaw, R. D.; Brinson, L. C.** (2003): Fiber waviness in nanotube-reinforced polymer composites - I: Modulus predictions using effective nanotube properties. *Compos Sci Tech*, vol. 63, no. 11, pp. 1689–1703.

**Fu, Y. H.; Klimkowski, K. J.; Rodin, G. J.; Berger, E.; Browne, J. C.; Singer, J. K.; Geijn, R. A.; Vernaganti, K. S.** (1998): A fast solution method for three-dimensional many-particle problems of linear elasticity. *Int J Numer Methods Engng*, vol. 42, pp. 1215–1229.

**Gong, X.; Liu, J.; Baskaran, S.; Voise, R. D.; Young, J. S.** (2000): Surfactant-assisted processing of carbon nanotube/polymer composites. *Chem Mater*, vol. 12, no. 4, pp. 1049–1052.

**Greengard, L.; Rokhlin, V.** (1997): A fast algorithm for particle simulations. *J Comput Phys*, vol. 135, pp. 280–292.

**Iijima, S.** (1999): Helical microtubules of graphitic carbon. *Nature*, vol. 354, pp. 56–58.

**Kimura, T.; Ago, H.; Tobita, M.; Ohshima, S.; Kyotani, M.; Yumura, M.** (2002): Polymer composites of carbon nanotubes aligned by a magnetic field. *Adv Mater*, vol. 14, no. 19, pp. 1380–1383.

**Ko, F.; Gogotsi, Y.; Ali, A.; Naguib, N.; Ye, H. H.; Yang, G. L.; Li, C.; Willis, P.** (2003): Electrospinning of continuous carbon nanotube-filled nanofiber yarns. *Adv Mater*, vol. 15, no. 14, pp. 1161–1165.

**Kong, F. Z.; Yao, Z. H.; Zheng, X. P.** (2002): BEM for simulation of a 2D elastic body with randomly distributed circular inclusions. *Acta Mech Solida Sinica*, vol. 15, no. 1, pp. 81–88.

**Liu, Y. J.; Chen, X. L.** (2003): Evaluations of the effective material properties of carbon nanotube-based composites using a nanoscale representative volume element. *Mechanics of Materials*, vol. 35, pp. 69–81.

**Liu, Y. J.; Nishimura, N.; Otani, Y.** (2005): Large-scale modeling of carbon-nanotube composites by a fast multipole boundary element method. *Computational Materials Science*, vol. 34, no. 2, pp. 173–187.

**Liu, Y. J.; Nishimura, N.; Otani, Y.; Takahashi, T.; Chen, X. L.; Munakata, H.** (2005): A fast boundary element method for the analysis of fiber-reinforced composites based on a rigid-inclusion model. *J Appl Mech*, vol. 72, no. 1, pp. 115–128.

**Nan, C. W.; Shi, Z.; Lin, Y.** (2003): A simple model for thermal conductivity of carbon nanotube-based composites. *Chem Phys Lett*, vol. 375, no. 5-6, pp. 666–669.

**Nishimura, N.; Yoshida, K.; Kobayashi, S.** (1999): A fast multipole boundary integral equation method for crack problems in 3D. *Engrg Anal Boundary Elements*, vol. 23, pp. 97–105.

**Nishimura, N.** (2002): Fast multipole accelerated boundary integral equation methods. *Appl Mech Rev*, vol. 55, no. 4, pp. 299–324.

**Nishimura, N.; Liu, Y. J.** (2004): Thermal analysis of carbon-nanotube composites using a rigid-line inclusion model by the boundary integral equation method. *Comput Mech*, vol. 35, pp. 1–10.

**Odegard, G. M.; Gates, T. S.; Wise, K. E.; Park, C.; Siochi, E. J.** (2003): Constitutive modeling of nanotube-reinforced polymer composites. *Compos Sci Tech*, vol. 63, no. 11, pp. 1671–1687.

**Popov, V. N.** (2004): Carbon nanotubes: properties and application. *Materials Science and Engineering R-Reports*, vol. 43, no. 3, pp. 61–102.

**Qian, D.; Dickey, E. C.; Andrews, R.; Rantell, T.** (2000): Load transfer and deformation mechanisms in carbon nanotube-polystyrene composites. *Appl Phys Lett*, vol. 76, pp. 2868–2870.

**Ryan, K. P.; Cadek, M.; Nicolosi, V.; Blond, D.; Ruether, M.; Armstrong, G.; Swan, H.; Fonseca, A.; Nagy, J. B.; Maser, W. K.; Blau, W. J.; Coleman, J. N.** (2007): Carbon nanotubes for reinforcement of plastics? A case study with poly(vinyl alcohol). *Composites Science and Technology*, vol. 67, pp. 1640–1649.

**Schadler, L .S.; Giannaris, S. C.; Ajayan, P. M.** (1998): Load transfer in carbon nanotube epoxy composites. *Appl Phys Lett*, vol. 73, no. 26, pp.

3842–3844.

**Shaffer, M. S. P.; Windle, A. H.** (1999): Fabrication and characterization of carbon nanotube/poly(vinyl alcohol) composites. *Adv Mater*, vol. 11, no. 11, pp. 937–941.

**Shen, L.; Liu, Y. J.** (2007): An adaptive fast multipole boundary element method for three-dimensional potential problems. *Comput Mech*, vol. 39, pp. 681–691.

**Singh, I. V.; Tanaka, M.; Endo, M.** (2007): Thermal analysis of CNT-based nano-composites by element free Galerkin method. *Computational Mechanics*, vol. 39, no. 6, pp. 719–728.

**Thostenson, E. T.; Chou, T. W.** (2002): Aligned multi-walled carbon nanotube-reinforced composites: processing and mechanical characterization. *J Phys D: Appl Phys*, vol. 35, no. 16, pp. L77–80.

**Thostenson, E. T.; Chou, T. W.** (2003): On the elastic properties of carbon nanotube-based composites: modeling and characterization. *J Phys D: Appl Phys*, vol. 36, pp. 573–582.

**Treacy, M. M. J.; Ebbesen, T. W.; Gibson, J.M.** (1996): Exceptionally high Young's modulus observed for individual carbon nanotubes. *Nature*, vol. 381, no. 6584, pp. 678–680.

**Wang, H. T.; Lei, T.; Li, J.; Huang, J. F.; Yao, Z. H.** (2007): A parallel fast multipole accelerated integral equation scheme for 3D Stokes equations. *International Journal for Numerical Methods in Engineering*, vol. 70, no. 7, pp. 812–839.

**Wang, H. T.; Yao, Z. H.** (2005): A new fast multipole boundary element method for large scale analysis of mechanical properties in 3-D particle-reinforced composites. *CMES: Computer Modeling in Engineering & Sciences*, vol. 7, no. 1, pp. 85–95.

**Wang, H. T., Yao, Z. H., Wang, P. B.** (2005): On the preconditioners for fast multipole boundary element methods for 2D multi-domain elastostatics. *Engineering Analysis with Boundary Elements*, vol. 29, no. 7, pp. 673–688.

**Weisenberger, M. C.; Grulke, E. A.; Jacques, D.; Rantell, T.; Andrews, R.** (2003): Enhanced mechanical properteis of polyacrylonitrile/multiwall carbon nanotube composite fibers. *Journal of Nanoscience and Nanotechnology*, vol. 3, no. 6, pp. 535–539.

**Yao, Z. H.; Kong, F. Z.; Wang, H. T.; Wang, P. B.** (2004): 2D Simulation of composite materials using BEM. *Engineering Analysis with Boundary Elements*, vol. 28, pp. 927–935.

**Yoshida, K., Nishimura, N.; Kobayashi, S.** (2001): Application of fast multipole Galerkin boundary integral equation method to crack problems in 3D. *Int J Numer Methods Engrg*, vol. 50, pp. 525–547.

**Yu, M.; Lourie, O.; Dyer, M. J.; Moloni, K.; Kelly, T. F.; Ruoff, R. S.** (2000): Strength and breaking mechanism of multiwalled carbon nanotubes under tensile load. *Science*, vol. 287, no. 5453, pp. 637–640.

**Zhu, L. J.; Narh, K. A.** (2004): Numerical simulation of the effect of nanotube orientation on tensile modulus of carbon-nanotube-reinforced polymer composites. *Polym Int*, vol. 53, no. 10, pp. 1461–1466.